JOURNAL OF GEOPHYSICAL RESEARCH, VOL. 116, A11313, doi:10.1029/2011JA016716, 2011

Confining the angular distribution of terrestrial gamma ray flash emission

T. Gjesteland,[1] N. Østgaard,[1] A. B. Collier,[2,3] B. E. Carlson,[1] M. B. Cohen,[4] and N. G. Lehtinen[4]

Received 1 April 2011; revised 29 August 2011; accepted 29 August 2011; published 11 November 2011.

[1] Terrestrial gamma ray flashes (TGFs) are bremsstrahlung emissions from relativistic electrons accelerated in electric fields associated with thunder storms, with photon energies up to at least 40 MeV, which sets the lowest estimate of the total potential of 40 MV. The electric field that produces TGFs will be reflected by the initial angular distribution of the TGF emission. Here we present the first constraints on the TGF emission cone based on accurately geolocated TGFs. The source lightning discharges associated with TGFs detected by RHESSI are determined from the Atmospheric Weather Electromagnetic System for Observation, Modeling, and Education (AWESOME) network and the World Wide Lightning Location Network (WWLLN). The distribution of the observation angles for 106 TGFs are compared to Monte Carlo simulations. We find that TGF emissions within a half angle >30° are consistent with the distributions of observation angle derived from the networks. In addition, 36 events occurring before 2006 are used for spectral analysis. The energy spectra are binned according to observation angle. The result is a significant softening of the TGF energy spectrum for large (>40°) observation angles, which is consistent with a TGF emission half angle (<40°). The softening is due to Compton scattering which reduces the photon energies.

Citation: Gjesteland, T., N. Østgaard, A. B. Collier, B. E. Carlson, M. B. Cohen, and N. G. Lehtinen (2011), Confining the angular distribution of terrestrial gamma ray flash emission, *J. Geophys. Res.*, *116*, A11313, doi:10.1029/2011JA016716.

1. Introduction

[2] TGFs are short (~1 ms) gamma emissions from the Earth's atmosphere. They were first observed by the Burst and Transient Source experiment (BATSE) on board the Compton Gamma Ray Observatory (CGRO) [*Fishman et al.*, 1994]. These gamma bursts have also been observed by other low Earth orbiting satellites such as the Reuven Ramaty High Energy Solar Spectroscopic Imager (RHESSI) [*Smith et al.*, 2005], AGILE [*Marisaldi et al.*, 2010] and Fermi [*Briggs et al.*, 2010]. TGFs are believed to be bremsstrahlung photons from relativistic electrons accelerated by runaway breakdown processes, a theory suggested nearly a century ago by *Wilson* [1924] and further developed in the 1990s [*Gurevich et al.*, 1992; *Roussel-Dupré et al.*, 1994; *Gurevich et al.*, 1996; *Lehtinen et al.*, 1996]. There is a strong connection between TGFs and thunderstorm activity, and the TGFs are found to occur in association with lightning discharges [*Inan et al.*, 1996; *Cummer et al.*, 2005; *Cohen et al.*, 2006; *Stanley et al.*, 2006; *Cohen et al.*, 2010b; *Shao et al.*, 2010].

[3] Several studies have analyzed the spectral properties of TGFs in order to determine the production altitude and initial angular emission. *Dwyer and Smith* [2005] analyzed RHESSI measurements and found they were best represented by 15 km production altitude and a gamma emission within 45° to vertical, or a narrow vertical gamma beam produced at 21 km. These results were later confirmed by *Carlson et al.* [2007], who also showed that a combined spectrum of the BATSE TGFs was consistent with a 15 km production altitude. *Østgaard et al.* [2008] analyzed each BATSE TGF separately and found that most TGFs were produced at 10–20 km altitude with a significant portion at higher altitudes (30–40 km). It was then shown by *Grefenstette et al.* [2008] that the BATSE instrument was saturated due to deadtime issues in the readout electronics. Motivated by these findings, *Gjesteland et al.* [2010] re-analyzed some of the TGFs that were thought to originate from high altitude (30–40 km) and found that the effect of deadtime saturation made the energy spectrum softer and therefore resulted in a too high production altitude. When deadtime was treated properly the estimated TGF production altitude was found to be 10–20 km in agreement with other studies. This means that both results

[1] Department of Physics and Technology, University of Bergen, Norway.
[2] SANSA Space Science, Hermanus, South Africa.
[3] School of Physics, University of KwaZulu-Natal, Durban, South Africa.
[4] Department of Electrical Engineering, Stanford University, Stanford, California, USA.

0148-0227/11/2011JA016716

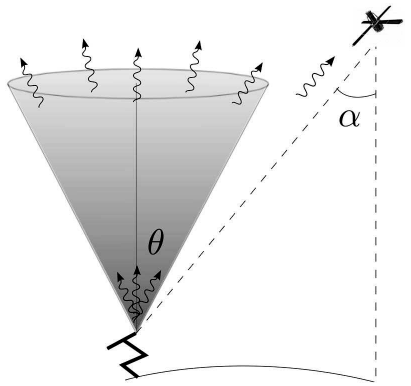

Figure 1. A sketch of the TGF emission cone with half angle θ and the satellite's observation angle α.

from average spectra and single spectrum analysis indicate TGF production ≤20 km.

[4] With a production altitude of 10–20 km, TGFs originate in the upper troposphere, probably inside thunderclouds. Based on gamma-photon attenuation in the atmosphere, *Williams et al.* [2006] suggested that high altitude intracloud lightning is the most likely source of TGFs. Cloud-to-ground lightning could also produce TGFs, however these TGFs are not likely to make it through the atmosphere due to attenuation [*Williams et al.*, 2006].

[5] TGFs are produced by acceleration of electrons in electrical fields that exceeds the runaway threshold. The electrical fields could be between charge regions in thunder clouds or in the strong electric field near leader tips. To gain the high number of electrons needed to produce a detectable TGF, *Dwyer* [2003] showed that positrons and photons may backscatter and create secondary avalanches leading to a true breakdown i.e. a breakdown which is self-sustained and do not need continues seeding to sustain the runaway process. *Moore et al.* [2001] have found energetic radiation associated with lightning stepped-leaders and *Moss et al.* [2006] have shown that streamers can produce enough relativistic seed electrons by acceleration of thermal electrons, such that the TGFs can be produced without feedback effects. *Carlson et al.* [2009, 2010] have shown that it is possible for electrons to be accelerated in the electric field near a leader tip. With seeding, as calculated by *Moss et al.* [2006], the field in leader tips is strong enough to produce TGFs. The electric field in the leader tip is divergent, implying that the TGF emission should be broad with a full width half maximum at half angle ~40° [*Carlson et al.*, 2010, Figure 1f].

[6] The geometry of the initial gamma emission is sketched in Figure 1. In the following we assume a vertical directed gamma emission within a cone given by half angle denoted θ, and the angle between the satellite nadir and the straight line to the TGF source α. The nature of the initial gamma emission is still under debate. Both *Dwyer and Smith* [2005] and *Carlson et al.* [2007] suggested a wide (θ = 45°) emission cone. *Østgaard et al.* [2008] found a softening of the TGF energy spectrum at increasing α which was also found in Monte Carlo (MC) simulations for TGFs observed outside the emission cone. The softening at increasing α was shown to be a result of Compton scattering. When the satellite observes TGFs outside the emission cone only scattered photons are detected. Scattering of photons reduces their energy and therefore leads to a softer energy spectrum. *Hazelton et al.* [2009] used lightning data from the World Wide Lightning Location Network (WWLLN) to divide TGFs into two groups, close and distant, according to whether or not TGFs were observed in association with lightning-producing storms closer than 300 km from the RHESSI sub-satellite point, which corresponds to an observation angle of $\alpha \sim 30°$ when the satellite is at ~600 km altitude. In their study they assumed a narrow and a wide TGF emission. The narrow emission cone was derived from MC simulations in a vertical electric field. The emission intensity (photons/sr) drops one order of magnitude at $\theta \sim 30°$ off axis. To simulate the effect of a divergent electric field, this emission cone was artificially broadened by convolving it with a Gaussian in solid angle. *Hazelton et al.* [2009] found that the wide emission cone provided the best fit to RHESSI data. They also reported 4 distant TGFs where the source lightning was geolocated. They all contained high energy photons ($E > 1$ MeV), which was consistent with their simulations of the broad emission.

[7] This paper will discuss the angular distribution of photon emission in the production of TGFs. In section 2 we will discuss gamma photon production and propagation in the atmosphere to show that the angular distribution of the emission must reflect the direction of the electric field producing TGFs. In section 3 we compare the distribution of the observation angles of RHESSI TGFs with MC simulations. To understand the softening of energy at large α section 4 presents a spectral analysis of TGFs observed at ($\alpha > 40°$). The discussion and conclusions are presented in sections 5 and 6.

2. Bremsstrahlung and Gamma-Photon Propagation in the Atmosphere

[8] The motion of electrons is dictated by the electric and magnetic fields. When the electron collision frequency is much larger than the gyrofrequency, the electron motion is predominantly in the direction of the electric field. *Gurevich et al.* [1996] showed that this is valid at altitudes below 20 km, because the effect of the Earth's magnetic field is negligible.

[9] Bremsstrahlung emitted by relativistic electrons is predominantly in the direction of the electron momentum, as can be seen, e.g., from the Bethe-Heitler formula [*Koch and Motz*, 1959]. The electrons are accelerated in the direction of the electric field and Coulomb scattering will spread their motion into a cone. A MC simulation of relativistic breakdown in a uniform vertical electric field by *Hazelton et al.* [2009] produced a narrow angular gamma emission where the intensity decreases to one half at $\theta \sim 20°$ and one order of magnitude at ~30° of axis. Since gamma emission is in the direction of the electron momentum and the electron momenta are aligned close with the electric field, the initial emission cone of the TGF has to reflect the electric field direction.

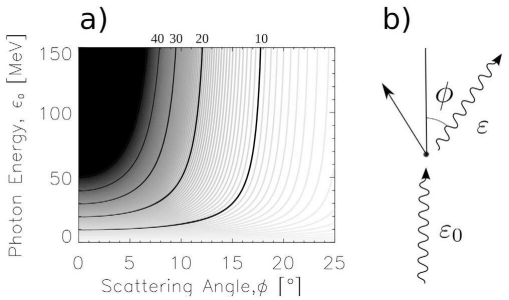

Figure 2. (a) Energy reduction as a function of scattering angle. Y-axis is the energy before scattering and the contour curves represent photon energy after Compton scattering: 10 MeV, 20 MeV, 30 MeV, and 40 MeV contours are labeled. (b) Compton scattering schematics.

[10] Gamma-photon flux propagating in air is attenuated, the most important interactions for photon energies in the range 10 keV–40 MeV being the photoelectric absorption, Compton scattering and pair production. Photoelectric absorption is almost negligible for photon energies above 100 keV and pair production is only effective for energies above 1.22 MeV. While in the photoelectric effect, the photons are absorbed with a production of an electron, in the pair production process, both an electron and a positron are created. Compton scattering is effective for all photon energies and results in scattering of the photon momentum and a loss in the photon energy. The reduction in photon energy is dramatic for large scattering angles. If the photon energy after scattering is 10 MeV it cannot have been scattered by more than 18°, assuming the photon energy before interaction is ≤150 MeV. Figure 2 shows the scattering angle, ϕ, as a function of initial photon energy, ε_0, when the photon energy after scattering, ε, is given. This relation is given by $\varepsilon = \varepsilon_0/(1 + \varepsilon(1 - \cos\phi)/m_e c^2$, where $m_e c^2$ = 511 keV. This is only valid for single Compton scattering events. By multiple scattering the energy reduction is not as dramatic and therefore Monte Carlo simulations are needed to validate the energy spectrum observed at large α.

3. Angular Distribution of TGFs Emission

[11] *Cohen et al.* [2010b] used the AWESOME network to determine the distance from the RHESSI sub-satellite point to the source lightning. A full description of AWESOME can be found in the work by *Cohen et al.* [2010a]. Thirty-six RHESSI TGFs were geolocated, 16 of which were geolocated with measurements from 3 or more stations, with 1σ uncertainty of ~30 km. The two-station cases have significantly larger uncertainties in their location and are therefore not included in this study.

[12] *Collier et al.* [2011] geolocated the source lightning of 93 RHESSI TGFs using WWLLN data, which has a spatial accuracy of 10 km [*Rodger et al.*, 2005]. Three of these TGFs were geolocated by both *Cohen et al.* [2010b] and *Collier et al.* [2011] and the sferic source locations were in agreement within the uncertainties [*Collier et al.*, 2011, Table 1]. This totals to 106 geolocated RHESSI TGFs available for this study. We assume that the TGFs are emitted at the same place and same time as the geolocated sferic. The uncertainties in timing between the sferics and TGFs are dominated by the uncertainties in the RHESSI clock which is assumed to be 1 or 2 ms [*Grefenstette et al.*, 2009]. The uncertainties in sferic timing is >50μs for AWESOME [*Cohen et al.*, 2010b] and 30μs for WWLLN [*Jacobson et al.*, 2006]. We have no information about which type of lightning the geolocated sferics comes from.

[13] The TGF angular distribution from these measurements is compared to calculated angle distributions using the code presented by *Østgaard et al.* [2008]. In this code, the production altitude, TGFs emission direction and energy spectrum are specified as initial conditions. With a production altitude of 15 km, energy spectrum $dN/dE \propto 1/E$ and gamma emission within a cone with half angle θ, Figure 3 shows the calculated scaling factor, $f(\alpha)$, between the initial number of photons, n_0, and the fluence going through a given area at satellite altitude, n_{sat}, as a function of observation angle, α:

$$n_{sat} = n_0 f(\alpha). \quad (1)$$

In Figure 3 all curves are normalized such that $f(0) = 1$. The different curves correspond to various half angle of the initial TGF emission i.e. $\theta = 20°$ (dotted), $\theta = 40°$ (dashed) and $\theta = 60°$ (dash-dotted). The solid curve is proportional to the inverse of the distance squared, demonstrating the reduction in the fluence in the absence of attenuation, referred to as the R^2-effect. Figure 3 shows that atmospheric attenuation reduces the fluence significantly more than the R^2-effect as the observation angle increases. For $\theta = 20°$ the fluence drops by a factor of ~4 if the observations are outside the emission cone. For $\theta = 40°$ the fluence also drops when the observations are outside the emission cone. At $\alpha = 60°$ the fluence has been reduced by more than one order of magnitude for all values of emission breadth θ.

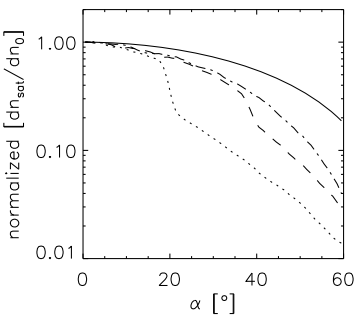

Figure 3. The scaling factor between the number of photons produced in a TGF and the number of photons detected by a satellite calculated by MC simulation. Production altitude is 15 km and $\theta = 20°$ (dotted), $\theta = 40°$ (dashed), and $\theta = 60°$ (dash–dotted). The R^2-effect is shown in solid. All curves are normalized so that $f(0) = 1$.

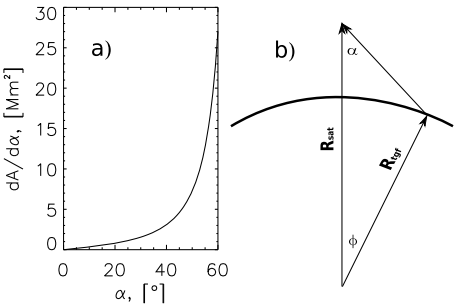

Figure 4. (a) The area as a function of α as given in equation (3). (b) A sketch of the geometry where $\mathbf{R_{SAT}}$ is from Earth's center to the satellite's position and $\mathbf{R_{TGF}}$ is from the Earth's center to the TGF origin.

[14] The number of TGFs per unit area detected by a satellite, $dN/d\alpha$, is given by the product of the area, $dA/d\alpha$, covered by the angle and the number of TGF per unit area exceed the threshold for detection, dN/dA, at that angle:

$$\frac{dN}{d\alpha} = \frac{dN}{dA}\frac{dA}{d\alpha}. \tag{2}$$

This is only valid when we assume that TGFs occur randomly in the satellite's field of view.

[15] A satellite orbiting the Earth covers a larger annular area as the observation angle increases. The area per unit angle in curved Earth geometry is given by:

$$\frac{dA}{d\alpha} = 2\pi R_{TGF}^2 \sin(\phi)\cdot\left(\frac{R_{SAT}}{R_{TGF}}\frac{\cos\alpha}{\cos(\phi+\alpha)} - 1\right), \tag{3}$$

where R_{TGF} and R_{SAT} are the distances from the Earth center to the TGFs origin and the satellite's position, ϕ is the angle between $\mathbf{R_{TGF}}$ and $\mathbf{R_{SAT}}$ given by $\phi = \sin^{-1}(\sin(\alpha)R_{SAT}/R_{TGF}) - \alpha$, $\alpha \in [0, \sin^{-1} R_{SAT}/R_{TGF})]$. $dA/d\alpha$ is shown in Figure 4a with a sketch of the geometry in Figure 4b. In the following we will derive $dN/d\alpha$.

[16] The number of TGF that can be detected at given angle is given by how many TGFs exceeding the threshold level for detection, n_{th}

$$\frac{dN}{dA} = \int_{n_{th}}^{\infty}\frac{dN}{dn_{sat}}dn_{sat}, \tag{4}$$

where dN/dn_{sat} is the distribution of TGFs versus number of photons detected by the satellite. The integral in (4) can be transformed to an integral over n_0 by substituting

$$\frac{dN}{dn_{sat}} = \frac{dN}{dn_0}\frac{dn_0}{dn_{sat}}, \tag{5}$$

where (1) gives $dn_0/dn_{sat} = 1/f(\alpha)$ and $dn_{sat} = f(\alpha)dn_0$. The lower integration limit changes to

$$n_{\min} = \frac{n_{th}}{f(\alpha)}, \tag{6}$$

where $n_{\min}$ is the lowest number of initial photons that will produce a detectable TGF. The upper limit remains at infinity. Substituting this into (4) yields

$$\frac{dN}{dA} = \int_{n_{\min}}^{\infty}\frac{dN}{dn_0}dn_0. \tag{7}$$

We assume that the initial number of photons in a TGF can be distributed according to a power law, which is shown to be feasible [*Collier et al.*, 2011]. Then the number of TGFs with n_0 initial photons are distributed according to

$$\frac{dN}{dn_0} \propto n_0^{-k}, \tag{8}$$

where k is the spectral index. We assume $1.5 < k < 3$. Solving (7) with the power law distribution gives

$$\frac{dN}{dA} \propto \frac{1}{k-1}\left(\frac{n_{th}}{f(\alpha)}\right)^{-k+1}, k > 1 \tag{9}$$

[17] The angular distribution $dN/d\alpha$ given in (2) with dN/dA from (9) and $dA/d\alpha$ from (3) will represent the angular distribution of TGF observations from Monte Carlo simulations for various values of k. Normalizing this distribution yields

$$\frac{dN(\alpha)}{d\alpha} \propto f(\alpha)^{k-1}dA/d\alpha. \tag{10}$$

[18] The distribution in (10), with $f(\alpha)$ from our simulations, are calculated for various k. For each k we have calculated the probability for (10) to represent the distribution of geolocated TGFs. The probability is calculated by a Kolmogorov-Smirnov two-sample test. The results are shown in Figure 5 for production altitudes 15 and 20 km. The three curves are for $\theta = 30°$ (solid), $\theta = 40°$ (dotted) and $\theta = 60°$ (dashed). The horizontal line shows a significance level of 0.05. For both 15 and 20 km production altitude and $\theta = 20°$ (not shown in Figure 5) the probability is below the significance level. From our analysis it follows that both $\theta = 30°$ and $\theta = 60°$ can represent the measured observation angle distribution. Emission cone with $\theta = 60°$ gives a higher spectral index, which means a softer distribution of initial photons, than an emission with $\theta = 30°$. As shown in Figure 5 our simulation only fit the measured distribution when $1.85 < k < 2.80$ for TGF produced at 15 km altitude and $1.90 < k < 2.85$ for TGF produced at 20 km.

[19] Figure 6 shows the observation angle distribution from the RHESSI measurements as a histogram. The best fit distribution from our simulations with various half angles is also shown. Half angle of $\theta = 30°$ with $k = 2.0$ is solid, $\theta = 40°$ with $k = 2.1$ is dotted and $\theta = 60°$ with $k = 2.3$ is dashed. The simulated distributions are normalized to the total number of observations in both *Cohen et al.* [2010b] and *Collier et al.* [2011]. For emission within $\theta = 30°$ our simulations show that most TGFs are detected when the satellite is within the emission cone ($\alpha \leq 30°$). When the satellite is outside the emission cone the number of observed TGF decreases significantly and only the initially brightest TGFs will be detected. An emission with $\theta = 40°$ will also

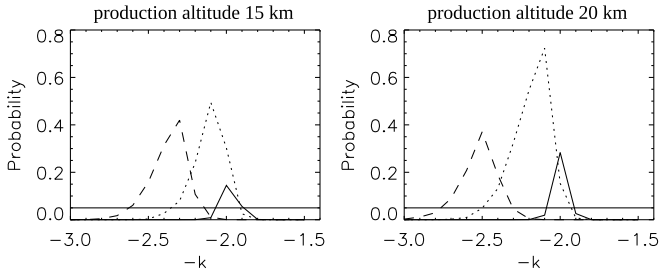

Figure 5. Probability for MC simulations to represent the observed TGF angle distribution for various spectral index, k. Various curves correspond to $\theta = 30°$ (solid), $\theta = 40°$ (dotted), and $\theta = 60°$ (dashed). The horizontal line represents a significant level of 0.05. When the probability is above this line the hypothesis cannot be rejected. TGF production altitude is given in the title of the plots.

give a decrease in number of detected TGFs as the satellite observes outside the emission cone. For $\theta = 60°$ all TGFs at satellite altitude will be detected within the emission cone. As shown in Figure 6 $\theta > 30°$ gives the best fit to the observed distribution.

4. Spectral Analysis of TGFs Observed at Large Angle ($\theta > 40°$)

[20] The energy spectrum of the TGFs can give us further information on the TGF emission cone. From the total set of the TGFs with corresponding geolocated sferics, 36 occurred before the radiation damage to the RHESSI instrument in early 2006 [*Grefenstette et al.*, 2009], and only events occurring before this are valid for proper spectral analysis. We have used the data and detector response matrix (DRM) from the RHESSI TGF catalog [*Grefenstette et al.*, 2009]. For each RHESSI TGF, the detected photons are too few (mean of 26) to perform spectral analysis. Therefore we have composited the measurements from these 36 TGFs into three spectra each with a 20° observation angle bin. Figure 7 shows each energy spectrum with the average number of counts and the error bars representing one standard deviation of the mean value. Figure 7 shows that RHESSI measures a significant softening of the energy spectrum in the 40°–60° bin versus the two others since the first energy bin has significantly more counts and the two highest energy bins have significantly fewer counts. There is also a trend that the 20°–40° spectrum is softer than the 0°–20° spectrum since it has significantly fewer counts in the highest energy bin.

[21] Figure 8 shows a combined energy spectrum of the 10 distant RHESSI TGFs. Distant TGFs are those detected at $\alpha > 40°$, which corresponds to ~500 km between the TGF production and the sub-satellite point. The simulated spectra in Figure 8 are results from our MC simulation folded through the RHESSI DRM. The initial half angle emission shown in Figure 8 is 30°, 40°, 50° and 60° and a production

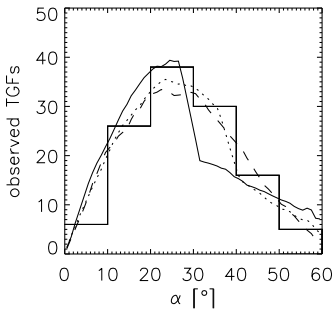

Figure 6. The histogram shows the distribution of geolocated TGFs per observation angle, α. The curves are the best results from MC simulations with $\theta = 30°$, $k = 2.0$ (solid); $\theta = 40°$, $k = 2.1$ (dotted); and $\theta = 60°$, $k = 2.3$ (dashed). The calculations were performed for the TGF source altitude of $h = 15$ km.

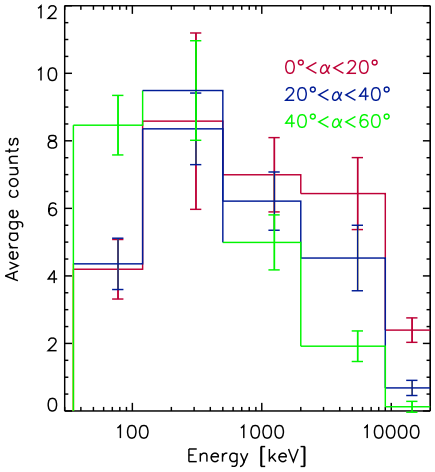

Figure 7. The average energy spectrum for various observation angles, α. The $40° < \alpha < 60°$ spectrum has significantly more counts in the lowest energy bin and significantly fewer counts in the two highest energy bins compared to the others.

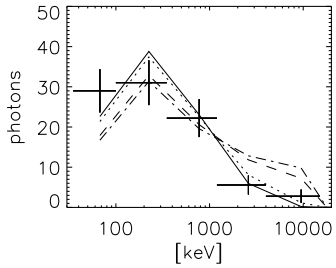

Figure 8. Combined energy spectrum from 10 distant ($\alpha > 40°$) RHESSI TGFs and the energy spectrum from MC simulations with $\theta = 30°$ (solid), $\theta = 40°$ (dotted), $\theta = 50°$ (dashed), and $\theta = 60°$ (dash–dotted). Production altitude of 15 km. The simulated spectra are normalized to the RHESSI measurements.

altitude of 15 km. The simulated spectra only contain photons that escape the atmosphere at $\alpha > 40°$. The simulated spectra are normalized to the combined RHESSI spectrum. The simulated spectra with $\theta \leq 40°$ are detected outside the emission cone. Therefore only scattered photons will be detected. This results in a softening of the energy spectrum. When the observation is obtained inside the emission cone ($\theta = 50°$ and $\theta = 60°$ in Figure 8) high energy photons may propagate directly from the TGF origin to the satellite. This would lead to a harder energy spectrum. In Figure 8 the combined RHESSI spectrum is significantly softer than the simulated spectra with $\theta = 50°$ and $\theta = 60°$, where the reduced χ^2-values are 1.91 ($p = 0.058$) and 2.36 ($p = 0.0108$). For $\theta = 30°$ and $\theta = 40°$ the simulated spectra have a closely matched softening to the combined RHESSI spectrum and the reduced χ^2-values are 0.64 ($p = 0.84$) and 0.84 ($p = 0.68$).

5. Discussion

[22] When calculating the observation angle distribution we have assumed a single TGF production altitude and a gamma emission where the number of photons emitted per solid angle is constant within the emission cone. With these assumptions we find that if TGFs have a narrow emission cone ($\theta = 20°$) the probability for our simulated distributions to represent the measured distribution is lower than a significance level of 0.05 for all values of k. As shown in Figure 5, an emission with $\theta = 30°$ has a peak probability of 0.15 for 15 km production altitude and 0.25 for 20 km production altitude. At both production altitudes the best spectral index is $k = 2.0$. Wider emission cones gives higher probability for our simulations to represent the data with a maximum at $\theta = 40°$. However, we cannot reject any of the hypotheses with $\theta \geq 30°$. An emission cone wider than 60° implies that all TGFs will be detected inside the emission cone and we can therefore not discuss the differences when $\theta > 60°$.

[23] For all emission cones we find that the spectral index should be in the range $1.85 < k < 2.8$ for production altitude 15 km and $1.9 < k < 2.85$ for 20 km. There are two important assumptions which may influence the results.

[24] 1. We have assumed a fixed production altitude. Several studies have shown that the TGF production altitude is in the range of ~14–20 km e.g. [*Smith et al.*, 2005; *Carlson et al.*, 2007; *Gjesteland et al.*, 2010]. Variation in the production altitude will change our constraints in both k and θ. However, since we get approximately similar results for both 15 km and 20 km, the constraints presented here should be valid for the range of most likely production altitudes.

[25] 2. We have assumed an isotropic emission within the cone. *Hazelton et al.* [2009] used an emission cone from MC simulations of runaway electrons. They show that photons emitted from bremsstrahlung in a non-divergent (uniform) electric field are spread with decreasing intensity to one half at $\theta \sim 20°$ and one order of magnitude at ~30° of axis. According to the simulations in the work by *Hazelton et al.* [2009] this is the narrowest emission cone possible from a relativistic runaway avalanche. This is consistent with $\theta \geq 30°$.

[26] Figure 7 shows significantly softer energy spectrum for TGFs observed at $\alpha = 40°–60°$ compared to TGFs observed at $\alpha = 0°–20°$ or $\alpha = 20°–40°$. The modeling results from *Østgaard et al.* [2008] have shown that TGFs sampled inside the emission cone will have a similar energy spectrum at all angles and a significant softening when the TGF is sampled outside the emission cone. This indicates that TGF observed at $\alpha = 40°–60°$ are outside the emission cone giving us a constraint that $\theta < 40°$.

[27] In a comparison with WWLLN geolocation of lightning associated with TGFs detected by Fermi Gamma Burst Monitor (GBM), *Connaughton et al.* [2010] found all 15 events to be observed within $\alpha \sim 30°$. *Cohen et al.* [2010b] and *Collier et al.* [2011] found that almost half of the TGFs are observed at $\alpha > 30°$. By comparing these results to MC simulations (see Figure 6), several TGFs observed at larger angles are consistent with simulation. The reason that GBM does not detect distant TGFs could be a result of differences in the trigger algorithm with respect to RHESSI or that GBM is less sensitive to TGFs with softer energy spectra. As shown in Figure 7, distant TGFs have a softer energy spectrum.

[28] The analysis of the angular distribution of TGFs emission (section 3) points toward an emission cone with $\theta \geq 30°$. The spectral analysis (section 4) indicates $\theta < 40°$. The range $30° < \theta < 40°$ is a little narrower than the half angle found in some earlier studies. *Dwyer and Smith* [2005] concluded that $\theta = 45°$ gave the best fit to the combined RHESSI spectrum and *Carlson et al.* [2007] concluded that $\theta \geq 45°$ could best represent the data.

[29] *Hazelton et al.* [2009] found that their wide emission cone, which had an intensity drop one order of magnitude at $\theta \sim 70°$ and 15 km production altitude, gave the lowest χ^2-value. However, they found that no single model (wide or narrow) fits all the data perfectly. *Hazelton et al.* [2009] separated TGFs into close and distant events. Close events are when there is lightning activity closer than 300 km from the sub-satellite point, which corresponds to $\alpha \sim 30°$. *Hazelton et al.* [2009] did not use detailed time coincidences between RHESSI and WWLLN events, but found plausible thunder storms.

[30] We found the half angle of the emission cone at $\theta \sim 40°$, therefore the distant energy spectrum in the work by

Hazelton et al. [2009] may include both direct and scattered TGFs photons. The inclusion of direct photons reduces the softening of the distant energy spectrum. A softer distant energy spectrum would fit better to their wide cone assumption [*Hazelton et al.*, 2009, Figure 1]. This indicates that an isotropic emission within $30° < \theta < 40°$ is comparable to the wide cone of *Hazelton et al.* [2009].

[31] *Carlson et al.* [2010] showed that if TGFs are produced by active lightning leader channels the gamma emission should be broad. The gamma emission predicted by *Carlson et al.* [2010, Figure 1f] drops one order of magnitude at $\theta \sim 90°$. The energy distribution of the photons emitted at large angles is not known. High energy photons emitted at large angles are not consistent with the softening of the energy spectrum found in this study.

[32] Our study indicates that the emissions are within $30° < \theta < 40°$. Assuming that the emission from a runaway breakdown in vertical electric field is emitted within $\theta \sim 20°$, which is where the intensity drops to one half in the simulation by *Hazelton et al.* [2009], our result suggest that TGFs are produced in electric fields that may have up to 20° deviation from vertical.

[33] In section 3 we assumed the TGF intensity to be distributed according to a power law and found the spectral index to be in the range $1.85 < k < 2.85$ for $\theta \geq 30°$. Since we confined the upper limit of the emission half angle to be $\theta \leq 40°$ our study indicates that the power law fit to the TGF intensity should have a spectral index $1.9 < k < 2.5$.

[34] RHESSI is known to suffer from deadtime [*Grefenstette et al.*, 2009] saturation. If TGFs saturates the detectors as much as they will not be detected the TGFs lost due to deadtime issues would be biased to short and bright TGFs [*Smith et al.*, 2010]. From our simulations the brightest TGFs are observed close to the sub satellite point. Both the R^2-effect and scattering and absorptions effects reduces the brightness at larger α. Simulations [*Gjesteland et al.*, 2010; *Grefenstette et al.*, 2008] showed that a TGF measured at larger α contain a Compton tail i.e. a tail of late arriving photons due to Compton scattering, which increase the TGF duration. Therefore, if RHESSI loses TGF due to deadtime it will manly lose TGFs at low α. If the distribution of detected TGFs are shifted to lower α that would imply a more narrow emission cone than presented in this study.

6. Summary

[35] We have used accurate geolocation of RHESSI TGFs to confine the angular TGF emission. When assuming an isotropic emission cone the half angle is confined to $30° < \theta < 40°$. This indicates that TGFs are produced in a vertical or nearly-vertical orientation (up to 20° from vertical) electric field.

[36] Our simulations shows that it is likely to detect TGFs at $\alpha > 50°$ which corresponds to >700 km between the source sferic and the sub-satellite point. We have also found that TGFs detected at $\alpha > 40°$ have a significantly softer energy spectrum, which has been interpreted to result from Compton scattering.

[37] Assuming that the total TGF intensities are distributed according to a power law (as suggested by *Collier et al.* [2011]), we confine the spectral index to $1.9 < k < 2.5$.

[38] **Acknowledgments.** This study was supported by the Research Council of Norway under contracts 184790/V30 and 197638/V30. Nikolai Lehtinen, Morris Cohen, and Brant Carlson would like to acknowledge support from NSF grant ATM-0836326. Nikolai Lehtinen would like to acknowledge support from DARPA grant HR0011-10-1-0058-P00001.

[39] Robert Lysak thanks the reviewers for their assistance in evaluating this manuscript.

References

Briggs, M. S., et al. (2010), First results on terrestrial gamma ray flashes from the Fermi Gamma-ray Burst Monitor, *J. Geophys. Res.*, *115*, A07323, doi:10.1029/2009JA015242.

Carlson, B. E., N. G. Lehtinen, and U. S. Inan (2007), Constraints on terrestrial gamma ray flash production from satellite observation, *Geophys. Res. Lett.*, *34*, L08809, doi:10.1029/2006GL029229.

Carlson, B. E., N. G. Lehtinen, and U. S. Inan (2009), Terrestrial gamma ray flash production by lightning current pulses, *J. Geophys. Res.*, *114*, A00E08, doi:10.1029/2009JA014531.

Carlson, B. E., N. G. Lehtinen, and U. S. Inan (2010), Terrestrial gamma ray flash production by active lightning leader channels, *J. Geophys. Res.*, *115*, A10324, doi:10.1029/2010JA015647.

Cohen, M. B., U. S. Inan, and G. Fishman (2006), Terrestrial gamma ray flashes observed aboard the Compton Gamma Ray Observatory/Burst and Transient Source Experiment and ELF/VLF radio atmospherics, *J. Geophys. Res.*, *111*, D24109, doi:10.1029/2005JD006987.

Cohen, M., U. Inan, and E. Paschal (2010a), Sensitive broadband ELF/VLF radio reception with the AWESOME instrument, *IEEE Trans. Geosci. Remote Sens.*, *48*(1), 3–17, doi:10.1109/TGRS.2009.2028334.

Cohen, M. B., U. S. Inan, R. K. Said, and T. Gjestland (2010b), Geolocation of terrestrial gamma-ray flash source lightning, *Geophys. Res. Lett.*, *37*, L02801, doi:10.1029/2009GL041753.

Collier, A. B., T. Gjesteland, and N. Østgaard (2011), Assessing the power law distribution of TGFs, *J. Geophys. Res.*, *116*, A10320, doi:10.1029/2011JA016612.

Connaughton, V., et al. (2010), Associations between Fermi Gamma-ray Burst Monitor terrestrial gamma ray flashes and sferics from the World Wide Lightning Location Network, *J. Geophys. Res.*, *115*, A12307, doi:10.1029/2010JA015681.

Cummer, S. A., Y. Zhai, W. Hu, D. M. Smith, L. I. Lopez, and M. A. Stanley (2005), Measurements and implications of the relationship between lightning and terrestrial gamma ray flashes, *Geophys. Res. Lett.*, *32*, L08811, doi:10.1029/2005GL022778.

Dwyer, J. R. (2003), A fundamental limit on electric fields in air, *Geophys. Res. Lett.*, *30*(20), 2055, doi:10.1029/2003GL017781.

Dwyer, J. R., and D. M. Smith (2005), A comparison between Monte Carlo simulations of runaway breakdown and terrestrial gamma-ray flash observations, *Geophys. Res. Lett.*, *32*, L22804, doi:10.1029/2005GL023848.

Fishman, G. J., et al. (1994), Discovery of intense gamma-ray flashes of atmospheric origin, *Science*, *264*, 1313–1316, doi:10.1126/science.264.5163.1313.

Gjesteland, T., N. Østgaard, P. H. Connell, J. Stadsnes, and G. J. Fishman (2010), Effects of dead time losses on terrestrial gamma ray flash measurements with the Burst and Transient Source Experiment, *J. Geophys. Res.*, *115*, A00E21, doi:10.1029/2009JA014578.

Grefenstette, B. W., D. M. Smith, J. R. Dwyer, and G. J. Fishman (2008), Time evolution of terrestrial gamma ray flashes, *Geophys. Res. Lett.*, *35*, L06802, doi:10.1029/2007GL032922.

Grefenstette, B. W., D. M. Smith, B. J. Hazelton, and L. I. Lopez (2009), First RHESSI terrestrial gamma ray flash catalog, *J. Geophys. Res.*, *114*, A02314, doi:10.1029/2008JA013721.

Gurevich, A. V., G. M. Milikh, and R. Roussel-Dupre (1992), Runaway electron mechanism of air breakdown and preconditioning during a thunderstorm, *Phys. Lett. A*, *165*, 463–468, doi:10.1016/0375-9601(92)90348-P.

Gurevich, A. V., J. A. Valdivia, G. M. Milikh, and K. Papadopoulos (1996), Runaway electrons in the atmosphere in the presence of a magnetic field, *Radio Sci.*, *31*(6), 1541–1554, doi:10.1029/96RS02441.

Hazelton, B. J., B. W. Grefenstette, D. M. Smith, J. R. Dwyer, X.-M. Shao, S. A. Cummer, T. Chronis, E. H. Lay, and R. H. Holzworth (2009), Spectral dependence of terrestrial gamma-ray flashes on source distance, *Geophys. Res. Lett.*, *36*, L01108, doi:10.1029/2008GL035906.

Inan, U. S., S. C. Reising, G. J. Fishman, and J. M. Horack (1996), On the association of terrestrial gamma-ray bursts with lightning and implications for sprites, *Geophys. Res. Lett.*, *23*(9), 1017–1020, doi:10.1029/96GL00746.

Jacobson, A. R., R. H. Holzworth, J. Harlin, R. L. Dowden, and E. H. Lay (2006), Performance assessment of the World Wide Lightning Location Network (WWLLN), using the Los Alamos Sferic Array (LASA) as

ground truth, *J. Atmos. Oceanic Technol.*, *23*, 1082–1092, doi:10.1175/JTECH1902.1.

Koch, H. W., and J. W. Motz (1959), Bremsstrahlung cross-section formulas and related data, *Rev. Mod. Phys.*, *31*(4), 920–955, doi:10.1103/RevModPhys.31.920.

Lehtinen, N. G., M. Walt, U. S. Inan, T. F. Bell, and V. P. Pasko (1996), γ-ray emission produced by a relativistic beam of runaway electrons accelerated by quasi-electrostatic thundercloud fields, *Geophys. Res. Lett.*, *23*(19), 2645–2648, doi:10.1029/96GL02573.

Marisaldi, M., et al. (2010), Detection of terrestrial gamma ray flashes up to 40 MeV by the AGILE satellite, *J. Geophys. Res.*, *115*, A00E13, doi:10.1029/2009JA014502.

Moore, C. B., K. B. Eack, G. D. Aulich, and W. Rison (2001), Energetic radiation associated with lightning stepped-leaders, *Geophys. Res. Lett.*, *28*(11), 2141–2144, doi:10.1029/2001GL013140.

Moss, G. D., V. P. Pasko, N. Liu, and G. Veronis (2006), Monte Carlo model for analysis of thermal runaway electrons in streamer tips in transient luminous events and streamer zones of lightning leaders, *J. Geophys. Res.*, *111*, A02307, doi:10.1029/2005JA011350.

Østgaard, N., T. Gjesteland, J. Stadsnes, P. H. Connell, and B. Carlson (2008), Production altitude and time delays of the terrestrial gamma flashes: Revisiting the Burst and Transient Source Experiment spectra, *J. Geophys. Res.*, *113*, A02307, doi:10.1029/2007JA012618.

Rodger, C. J., J. B. Brundell, and R. L. Dowden (2005), Location accuracy of VLF World-Wide Lightning Location (WWLL) network: Post-algorithm upgrade, *Ann. Geophys.*, *23*(2), 277–290.

Roussel-Dupré, R. A., A. V. Gurevich, T. Tunnell, and G. M. Milikh (1994), Kinetic theory of runaway air breakdown, *Phys. Rev. E*, *49*(3), 2257–2271, doi:10.1103/PhysRevE.49.2257.

Shao, X.-M., T. Hamlin, and D. M. Smith (2010), A closer examination of terrestrial gamma-ray flash-related lightning processes, *J. Geophys. Res.*, *115*, A00E30, doi:10.1029/2009JA014835.

Smith, D. M., L. I. Lopez, R. P. Lin, and C. P. Barrington-Leigh (2005), Terrestrial gamma-ray flashes observed up to 20 MeV, *Science*, *307*, 1085–1088, doi:10.1126/science.1107466.

Smith, D. M., B. J. Hazelton, B. W. Grefenstette, J. R. Dwyer, R. H. Holzworth, and E. H. Lay (2010), Terrestrial gamma ray flashes correlated to storm phase and tropopause height, *J. Geophys. Res.*, *115*, A00E49, doi:10.1029/2009JA014853.

Stanley, M. A., X.-M. Shao, D. M. Smith, L. I. Lopez, M. B. Pongratz, J. D. Harlin, M. Stock, and A. Regan (2006), A link between terrestrial gamma-ray flashes and intracloud lightning discharges, *Geophys. Res. Lett.*, *33*, L06803, doi:10.1029/2005GL025537.

Williams, E., et al. (2006), Lightning flashes conducive to the production and escape of gamma radiation to space, *J. Geophys. Res.*, *111*, D16209, doi:10.1029/2005JD006447.

Wilson, C. T. R. (1924), The electric field of a thundercloud and some of its effects, *Proc. Phys. Soc. London*, *37*, 32D–37D.

B. E. Carlson, T. Gjesteland, and N. Østgaard, Department of Physics and Technology, University of Bergen, Allegaten 55, N-5007 Bergen, Norway. (brant.carlson@ift.uib.no; thomas.gjesteland@uib.no; nikolai.ostgaard@uib.no)

M. B. Cohen and N. G. Lehtinen, Department of Electrical Engineering, Stanford University, 350 Serra Mall, Stanford, CA 94305, USA. (mcohen@stanford.edu; nleht@stanford.edu)

A. B. Collier, School of Physics, University of KwaZulu-Natal, Westville Campus, Durban 4000, South Africa. (collierab@gmail.com)